# Rotational bands in $^{133}$Ce

R. Ma, E. S. Paul, C. W. Beausang,* S. Shi,† N. Xu, and D. B. Fossan
*Department of Physics, State University of New York at Stony Brook, Stony Brook, New York 11794*
(Received 7 August 1987)

Several rotational bands built on one- and three-quasiparticle configurations have been populated in the odd-neutron $^{133}$Ce nucleus following the $^{119}$Sn($^{18}$O,4n) reaction. Both signature components of bands built on the $[514]\frac{9}{2}^-$ and $[400]\frac{1}{2}^+$ orbitals were observed. At low spins, the yrast band, based on a neutron from the upper $h_{11/2}$ midshell, shows a large signature splitting ($>100$ keV), indicating a significant triaxial deformation ($\gamma\sim-20°$). Four $\Delta I=1$ bands were observed at higher spins based on three-quasiparticle configurations. Strong $M1$ transitions and the lack of signature splitting imply that these bands are near prolate ($\gamma\sim0°$) and thus contain one or more aligned $h_{11/2}$ protons from the lower midshell. In two of these bands, weak $E2$ crossover transitions were seen; measured $B(M1;I\rightarrow I-1)/B(E2;I\rightarrow I-2)$ ratios were used to assign configurations. In addition, a $\Delta I=2$ band with an enhanced moment of inertia was observed most probably built on the prolate $\nu i_{13/2}\otimes[\pi h_{11/2}]^2$ configuration. Only one signature component of this configuration was seen because of the maximal signature splitting of the $\beta$-driving $i_{13/2}$ neutron orbital ($\Omega=\frac{1}{2}$).

## I. INTRODUCTION

A wealth of spectroscopic information is manifest in the properties of odd-neutron nuclei in the mass $A\sim130$ region. One interesting feature is the relation between the energy splitting of opposite signature components of rotational bands and the deviation of the nuclear shape away from axial symmetry, as represented by the shape asymmetry parameter $\gamma$. The $\nu h_{11/2}$ yrast bands of nuclei in this region exhibit large signature splittings at low rotational frequencies. The magnitude of the splitting, typically $\sim100$ keV, is much greater than predicted for the high-$\Omega$ neutron in a prolate nucleus ($\gamma=0°$, Lund convention[1]). This large signature splitting is taken as evidence for triaxial shapes ($\gamma\sim-20°$) in these nuclei at low spin. Prominent examples[2,3] of such odd-$N$ nuclei include $^{129}$Ce and $^{135}$Nd. It is the shape driving effect of the $h_{11/2}$ neutron, from the upper midshell, on the $\gamma$-soft core[4,5] that induces the triaxial deformation. A second feature that is sensitive to the nuclear shape $(\beta,\gamma)$ is the particle alignment frequency for specific nucleonic pairs. In this mass region, the degree of triaxiality $\gamma$ has a greater influence on the crossing frequencies than the quadrupole deformation $\beta$. Rotational alignments observed in the $\nu h_{11/2}$ bands are due to a pair of low-$\Omega$ $h_{11/2}$ protons from the lower midshell, the corresponding $h_{11/2}$ neutron aligment being blocked. The triaxial shape of these $h_{11/2}$ one-quasineutron bands increases the crossing frequency of the protons relative to that for similar crossings in prolate nuclei. A third structure feature in this mass region is the induced shape change caused by the additional $\gamma$-driving forces on the nuclear core by the aligned protons. The position of the Fermi surface within a high-$j$ shell determines[6] the value of $\gamma$ favored by the valence quasiparticles. In contrast to the high-$\Omega$ neutrons favoring triaxial shapes ($\gamma<0°$), the low-$\Omega$ protons drive to prolate shapes ($\gamma\sim0°$). Thus the rotational alignment of $h_{11/2}$ protons is associated with a shape change of the nucleus from a triaxial shape at low frequencies to a prolate shape at higher frequencies after the alignment. This shape change is again evident from the measured signature splitting in these bands which essentially falls to zero, as expected for the prolate shape. Similar shape changes induced by quasiparticle alignment ($\nu i_{13/2}$) in heavier $\gamma$-soft nuclei (Ho and Dy isotopes) have been discussed by Frauendorf and May[7] using the formalism of the cranked shell-model (CSM).[8] The present paper reports on the above properties in $^{133}$Ce and compares the results to those[3,9] of the heavier N=75 isotopes $^{135}$Nd and $^{137}$Sm.

In odd nuclei, electromagnetic properties, sensitive to specific configurations, can be easily obtained from measured intensity ratios of competing $M1$ and $E2$ transitions. In contrast, similar information is only obtained for even-even nuclei from more difficult lifetime measurements. In particular, the observation of both $\Delta I=1$ and $\Delta I=2$ transitions in the rotational bands of odd-$N$ nuclei allows the extraction of ratios of reduced transition probabilities $B(M1;I\rightarrow I-1)/B(E2;I\rightarrow I-2)$ from the measured branching ratios. Ratios have been extracted for bands in $^{133}$Ce and compared to calculations for various quasiparticle configurations using the semiclassical formalism[10] of Dönau and Frauendorf. In $^{133}$Ce both signatures of bands built on low-lying $I^\pi=\frac{9}{2}^-$ and $I^\pi=\frac{1}{2}^+$ states have been populated. In addition, four bands of strong $\Delta I=1$ transitions were seen at higher spins, most likely built on three-quasiparticle configurations. For two of these bands the $E2$ crossover transitions were observed, although only weakly. These bands have been assigned configurations by comparison of their measured and calculated $B(M1)/B(E2)$ ratios.

An additional band, consisting of $\Delta I=2$ transitions,

 

was observed to high spin in $^{133}$Ce. Because only one signature component was observed, this band must be built on a configuration containing a neutron in a low-$\Omega$ orbital for the expected near-prolate nuclear shape. From Nilsson single-particle systematics, the two possibilities for this mass region are the $f_{7/2}[541]\frac{1}{2}^-$ and the $i_{13/2}[660]\frac{1}{2}^+$ orbitals. This neutron is coupled to a pair of rotationally aligned $h_{11/2}$ protons.

## II. EXPERIMENTAL METHODS AND RESULTS

The high-spin states of $^{133}$Ce were populated using the $^{119}$Sn($^{18}$O,4n$\gamma$)$^{133}$Ce reaction at a bombarding energy of 75 MeV. The $^{18}$O ions were delivered by the Stony Brook Superconducting LINAC injected by the tandem Van de Graaff accelerator. The tin target consisted of 4 mg/cm$^2$ of $^{119}$Sn rolled onto a lead backing of thickness 50 mg/cm$^2$. Four n-type Ge detectors were used, each having an efficiency of 25% relative to a 7.6 cm$\times$7.6 cm NaI(Tl) detector for 1.3 MeV $\gamma$ rays. The detectors were located at $\pm$57° and $\pm$136° with respect to the beam direction, and at a distance of 17 cm from the target. Each of the four detectors utilized bismuth germanate (BGO) anti-Compton shields of the transverse type.[11]

Multiplicity information was also recorded using seven closely-packed hexagonal BGO crystals (5.1 cm$\times$15.2 cm long) positioned below the target in addition to four 7.6 cm$\times$7.6 cm NaI(Tl) crystals placed above the target. Transitions in $^{133}$Ce were enhanced relative to other background channels by demanding that two or more of the multiplicity elements fired in coincidence with at least two of the Compton-suppressed Ge detectors during playback of the tapes. Under these conditions, Coulex and activity lines were greatly reduced in the gated coincidence spectra.

Approximately 50 million double or higher order coincidence events were written onto tape, event by event for subsequent data analysis. The tapes were scanned offline (with the multiplicity requirement) on a VAX 11-780 computer to produce a symmetrized array of $E_\gamma$ vs $E_\gamma$. Background-subtracted gated spectra generated from this array were used to construct the decay scheme of $^{133}$Ce shown in Fig. 1. Examples of gated coincidence spectra are presented in Fig. 2 showing transitions assigned to some of the bands in $^{133}$Ce.

No angular distribution measurement was made for $^{133}$Ce; in practice, it has been found that because the singles spectra are so complex, the extraction of reliable angular distribution coefficients for many of the peaks is difficult. However, the coincidence data contain angular correlation information. A two-dimensional angular correlation array was created from the data with the $\pm$136° detectors as one axis and the $\pm$57° detectors as the other axis. Gated spectra generated from this array were used to obtain directional correlation[12] (DCO) intensity ratios $I(136°)/I(57°)$. Most of the ratios were obtained using the 619.7 keV $E2$ transition near the bottom of the $\nu h_{11/2}$ band (labeled 6 in Fig. 1) as the gating transition. In some cases, other $E2$ transitions were used as the gate, while for some of the weaker lines, the intensity ratio was obtained from total projected spectra from the array, projected onto the 136° and 57° axes. In effect, the gating window consists of the whole spectrum, i.e., $2k$ channels. Although this method has better

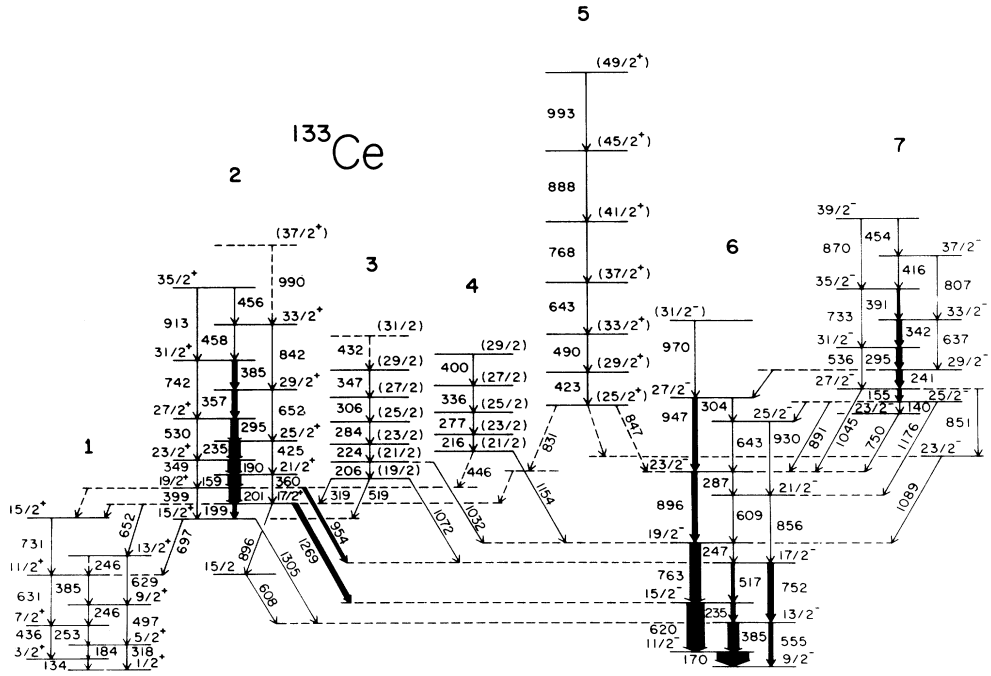


FIG. 1. Level scheme of $^{133}$Ce deduced from this work. The transition energies are given in keV and the widths of the arrows indicate their relative intensities. For clarity, some weak interband transitions are unlabeled.

statistics, the empirical intensity ratios obtained do not distinguish dipole transitions from quadrupole transitions as well as the ratios obtained using a gating quadrupole transition. The results of this analysis are presented in Table I together with the relative intensities of all the transitions assigned to $^{133}$Ce. In general, the angular correlation ratio is greater than 1.0 for stretched quadrupole transitions and less than 0.9 for stretched dipole transitions. The transition intensities have been corrected for the efficiency of the Ge detectors and also for internal conversion effects using the calculated conversion coefficients of Rösel *et al.*[13] The values have been normalized to the 619.7 keV $\frac{15}{2}^- \rightarrow \frac{11}{2}^-$ transitions of the $\nu h_{11/2}$ band.

A pulsed beam $E_\gamma$-$t$ measurement was also performed, with a duration of 106 ns between successive beam

TABLE I. Energies, intensities, and angular correlation data for transitions assigned to $^{133}$Ce. Except where indicated, the angular correlation intensity ratios were obtained from gated spectra using the 619.7 keV $E2$ transition as the gating transition.

| $E_\gamma$ (keV)[a] | $I_\gamma$[b] | $I(136°)/I(57°)$ | Assignment | $E_\gamma$ (keV)[a] | $I_\gamma$[b] | $I(136°)/I(57°)$ | Assignment |
|---|---|---|---|---|---|---|---|
| 134.0 | 3.9 | 0.88(03)[c] | $\frac{3}{2}^+ \rightarrow \frac{1}{2}^+$ | 454.4 | 6.6(7) | | $\frac{39}{2}^- \rightarrow \frac{37}{2}^-$ |
| 140.0 | 3.0 | 0.93(05)[c] | $\frac{25}{2}^- \rightarrow \frac{23}{2}^-$ | 456.5 | 12.6 | 0.62(16) | $\frac{35}{2}^+ \rightarrow \frac{33}{2}^+$ |
| 154.7 | 20.9 | 0.64(07) | $\frac{27}{2}^- \rightarrow \frac{25}{2}^-$ | 457.9 | | | $\frac{33}{2}^+ \rightarrow \frac{31}{2}^+$ |
| 159.5 | 70.5 | 0.70(01) | $\frac{21}{2}^+ \rightarrow \frac{19}{2}^+$ | 489.4 | 14.8(1.9) | 1.14(10)[d] | $(\frac{33}{2}^+ \rightarrow \frac{29}{2}^+)$ |
| 164.0 | <2.0 | | $\frac{17}{2}^+ \rightarrow \frac{15}{2}^+$ | 497.4 | <2.0 | | $\frac{9}{2}^+ \rightarrow \frac{5}{2}^+$ |
| 170.2 | 180.6 | 0.58(01) | $\frac{11}{2}^- \rightarrow \frac{9}{2}^-$ | 503.0 | 4.0 | | $(\frac{23}{2} \rightarrow \frac{21}{2}^+)$ |
| 183.5 | <2.0 | 0.74(05)[c] | $\frac{5}{2}^+ \rightarrow \frac{3}{2}^+$ | 516.8 | 22.9 | 0.54(04) | $\frac{17}{2}^- \rightarrow \frac{15}{2}^-$ |
| 189.5 | 67.4 | 0.66(01) | $\frac{23}{2}^+ \rightarrow \frac{21}{2}^+$ | 518.6 | <2.0 | | $(\frac{19}{2} \rightarrow \frac{15}{2}^+)$ |
| 198.8 | 10.5 | 0.77(04) | $\frac{17}{2}^+ \rightarrow \frac{15}{2}^+$ | 529.5 | 3.8 | | $\frac{27}{2}^+ \rightarrow \frac{23}{2}^+$ |
| 200.7 | 55.1 | | $\frac{19}{2}^+ \rightarrow \frac{17}{2}^+$ | 535.5 | 3.1(4) | | $\frac{31}{2}^- \rightarrow \frac{27}{2}^-$ |
| 205.5 | 10.4 | 0.60(14) | $(\frac{21}{2} \rightarrow \frac{19}{2})$ | 554.9 | 18.9 | 1.12(02)[c] | $\frac{13}{2}^- \rightarrow \frac{9}{2}^-$ |
| 215.5 | 7.7 | 0.85(02)[c] | $(\frac{23}{2} \rightarrow \frac{21}{2})$ | 608.5 | 16.7 | 0.69(10) | $\frac{15}{2} \rightarrow \frac{13}{2}^-$ |
| 223.6 | 11.1 | 0.79(11) | $(\frac{23}{2} \rightarrow \frac{21}{2})$ | 609.5 | 8.0 | | $\frac{21}{2}^- \rightarrow \frac{19}{2}^-$ |
| 234.9 | 24.9 | 0.72(04) | $\frac{15}{2}^- \rightarrow \frac{13}{2}^-$ | 619.7 | ≡100.0 | 1.16(01)[c] | $\frac{15}{2}^- \rightarrow \frac{11}{2}^-$ |
| 235.0 | 55.0 | | $\frac{25}{2}^+ \rightarrow \frac{23}{2}^+$ | 629.4 | 3.4 | 1.82(14)[c] | $\frac{13}{2}^+ \rightarrow \frac{9}{2}^+$ |
| 240.6 | 34.4 | 0.68(04) | $\frac{29}{2}^- \rightarrow \frac{27}{2}^-$ | 630.5 | | | $\frac{11}{2}^+ \rightarrow \frac{7}{2}^+$ |
| 246.5 | 12.6 | 0.76(14) | $\frac{19}{2}^- \rightarrow \frac{17}{2}^-$ | 636.9 | 4.5 | | $\frac{33}{2}^- \rightarrow \frac{29}{2}^-$ |
| 253.0 | 2.8 | 0.79(06)[c] | $\frac{7}{2}^+ \rightarrow \frac{5}{2}^+$ | 643.0 | 14.7(1.9) | 1.09(12)[d] | $(\frac{37}{2}^+ \rightarrow \frac{33}{2}^+)$ |
| 276.5 | 9.5 | 0.70(19) | $(\frac{25}{2} \rightarrow \frac{23}{2})$ | 651.5 | | 1.30(12)[c] | $\frac{17}{2}^+ \rightarrow \frac{13}{2}^+$ |
| 283.5 | 11.0 | 0.69(09) | $(\frac{25}{2} \rightarrow \frac{23}{2})$ | 652.0 | 3.8 | | $\frac{29}{2}^+ \rightarrow \frac{25}{2}^+$ |
| 287.0 | <2.0 | | $\frac{23}{2}^- \rightarrow \frac{21}{2}^-$ | 697.0 | <2.0 | | $\frac{15}{2}^+ \rightarrow \frac{11}{2}^+$ |
| 294.6 | 32.7 | 0.75(03) | $\frac{27}{2}^+ \rightarrow \frac{25}{2}^+$ | 731.0 | <2.0 | | $\frac{15}{2}^+ \rightarrow \frac{11}{2}^+$ |
| 294.9 | 28.6 | | $\frac{31}{2}^- \rightarrow \frac{29}{2}^-$ | 733.5 | 5.5 | | $\frac{35}{2}^- \rightarrow \frac{31}{2}^-$ |
| 304.0 | <2.0 | | $\frac{27}{2}^- \rightarrow \frac{25}{2}^-$ | 742.0 | 5.0 | 1.20(46) | $\frac{31}{2}^+ \rightarrow \frac{27}{2}^+$ |
| 305.7 | 4.4 | | $(\frac{27}{2} \rightarrow \frac{25}{2})$ | 751.2 | 33.0 | 1.17(02)[c] | $\frac{17}{2}^- \rightarrow \frac{13}{2}^-$ |
| 318.0 | 2.5(3) | | $\frac{5}{2}^+ \rightarrow \frac{1}{2}^+$ | 762.7 | 52.1 | 1.03(05) | $\frac{19}{2}^- \rightarrow \frac{15}{2}^-$ |
| 319.6 | <2.0 | | $(\frac{19}{2} \rightarrow \frac{17}{2}^+)$ | 767.5 | 6.8(9) | 1.10(17)[d] | $(\frac{41}{2}^+ \rightarrow \frac{37}{2}^+)$ |
| 335.5 | 6.1 | | $(\frac{27}{2} \rightarrow \frac{25}{2})$ | 806.8 | 3.0 | | $\frac{37}{2}^- \rightarrow \frac{33}{2}^-$ |
| 338.0 | <2.0 | | $\frac{29}{2}^- \rightarrow \frac{27}{2}^-$ | 831.1 | 2.3 | | $\frac{25}{2}^+ \rightarrow$ |
| 342.0 | 22.8 | 0.69(09) | $\frac{33}{2}^- \rightarrow \frac{31}{2}^-$ | 842.4 | <2.0 | | $\frac{33}{2}^+ \rightarrow \frac{29}{2}^+$ |
| 346.5 | 2.3 | 0.73(03)[c] | $(\frac{29}{2} \rightarrow \frac{27}{2})$ | 847.1 | 4.3 | 0.85(04)[c] | $\frac{25}{2}^+ \rightarrow \frac{23}{2}^-$ |
| 349.0 | <2.0 | | $\frac{23}{2}^+ \rightarrow \frac{19}{2}^+$ | 851.0 | <2.0 | 1.13(07)[c] | $\frac{27}{2}^- \rightarrow \frac{23}{2}^-$ |
| 357.5 | 22.3 | 0.72(08) | $\frac{29}{2}^+ \rightarrow \frac{27}{2}^+$ | 856.0 | 7.9 | 1.22(27) | $\frac{21}{2}^- \rightarrow \frac{17}{2}^-$ |
| 360.0 | <2.0 | | $\frac{21}{2}^+ \rightarrow \frac{17}{2}^+$ | 870.5 | 3.1 | 1.08(27) | $\frac{39}{2}^- \rightarrow \frac{35}{2}^-$ |
| 384.5 | 23.4 | 0.54(08) | $\frac{31}{2}^+ \rightarrow \frac{29}{2}^+$ | 888.0 | <2.0 | 1.05(20)[d] | $(\frac{45}{2}^+ \rightarrow \frac{41}{2}^+)$ |
| 384.7 | 51.0 | | $\frac{13}{2}^- \rightarrow \frac{11}{2}^-$ | 890.5 | <2.0 | 1.58(06)[c] | $\frac{25}{2}^- \rightarrow \frac{23}{2}^-$ |
| 391.1 | 12.4 | 0.48(11) | $\frac{35}{2}^- \rightarrow \frac{33}{2}^-$ | 896.0 | 33.4 | 1.02(08) | $\frac{23}{2}^- \rightarrow \frac{19}{2}^-$ |
| 399.4 | <2.0 | 1.04(36) | $\frac{19}{2}^+ \rightarrow \frac{15}{2}^+$ | 896.4 | 4.6 | | $\frac{17}{2}^+ \rightarrow \frac{15}{2}$ |
| 400.1 | | | $(\frac{29}{2} \rightarrow \frac{27}{2})$ | 913.3 | 1.7 | 1.29(21)[c] | $\frac{35}{2}^+ \rightarrow \frac{31}{2}^+$ |
| 415.6 | 6.9 | 0.45(03)[c] | $\frac{37}{2}^- \rightarrow \frac{35}{2}^-$ | 930.0 | 3.9 | | $\frac{25}{2}^- \rightarrow \frac{21}{2}^-$ |
| 423.1 | 10.5(1.3) | 1.06(17) | $(\frac{29}{2}^+ \rightarrow \frac{25}{2}^+)$ | 946.9 | 24.6 | 1.03(18) | $\frac{27}{2}^- \rightarrow \frac{23}{2}^-$ |
| 424.5 | 2.3(4) | | $\frac{25}{2}^+ \rightarrow \frac{21}{2}^+$ | 954.0 | 22.5 | 0.51(09) | $\frac{19}{2}^+ \rightarrow \frac{17}{2}^-$ |
| 432.0 | <2.0 | | $(\frac{31}{2} \rightarrow \frac{29}{2})$ | 971.0 | 4.6 | | $\frac{31}{2}^- \rightarrow \frac{27}{2}^-$ |
| 436.1 | 3.1 | 0.90(07)[c] | $\frac{7}{2}^+ \rightarrow \frac{3}{2}^+$ | 993.0 | <2.0 | | $(\frac{49}{2}^+ \rightarrow \frac{45}{2}^+)$ |

TABLE I. (*Continued*).

| $E_\gamma$ (keV)[a] | $I_\gamma$[b] | $I(136°)/I(57°)$ | Assignment | $E_\gamma$ (keV)[a] | $I_\gamma$[b] | $I(136°)/I(57°)$ | Assignment |
|---|---|---|---|---|---|---|---|
| 1031.5 | <2.0 | 0.57(33) | $(\frac{21}{2}\rightarrow\frac{19}{2}^-)$ | 1154.0 | <2.0 | | $(\frac{21}{2}\rightarrow\frac{19}{2}^-)$ |
| 1045.4 | 8.3 | 1.05(24) | $\frac{27}{2}^-\rightarrow\frac{23}{2}^-$ | 1176.5 | 5.5 | 1.72(57) | $\frac{25}{2}^-\rightarrow\frac{21}{2}^-$ |
| 1071.6 | 5.8 | 0.78(28) | $(\frac{19}{2}\rightarrow\frac{17}{2}^-)$ | 1269.3 | 27.1 | 0.91(06) | $\frac{17}{2}^+\rightarrow\frac{15}{2}^-$ |
| 1089.0 | <2.0 | 1.89(37)[c] | $\frac{23}{2}^-\rightarrow\frac{19}{2}^-$ | 1305.4 | 5.5 | 1.09(05)[c] | $\frac{15}{2}^+\rightarrow\frac{13}{2}^-$ |

[a]The energies are accurate to ±0.2 keV for the stronger transitions rising to ±0.5 keV for the weak transitions.
[b]The transition intensities were obtained from a combination of total projection and gated spectra generated from the $E_\gamma$-$E_\gamma$ data array. Except where stated, errors on these intensities are less than 10%.
[c]Angular intensity ratio obtained from total projections of correlation matrix.
[d]Angular intensity ratio obtained from gated spectrum, using the 423.1 keV quadrupole transition as the gate.

pulses. From these data it was possible to place an upper limit of $t_{1/2}<8$ ns for the nuclear levels of $^{133}$Ce presented in Fig. 1, except for the low-lying $\frac{1}{2}^+$ and $\frac{9}{2}^-$ bandheads which have previously measured[14] lifetimes of 97 min and 4.9 h, respectively.

## III. DISCUSSION

### A. Experimental alignments and routhians

In order to discuss the rotational properties of the nucleus, it is appropriate to transform the experimental data into the intrinsic body-fixed frame. This is achieved following the procedures of Bengtsson and Frauendorf[8] to produce the experimental alignments and routhians ($i_x$ and $e'$). Such alignments

$$i_x = I_x - I_{x,\mathrm{ref}} , \tag{1}$$

and routhians

$$e' = E - \hbar\omega I_x + \hbar \int I_{x,\mathrm{ref}} d\omega , \tag{2}$$

of most of the bands in $^{133}$Ce are shown in Fig. 3. In the preceding equations, $I_x$ is the projection of the total spin on the rotation axis, while $I_{x,\mathrm{ref}}$ is a reference based on a frequency-dependent moment of inertia[15] $\mathcal{J}_{\mathrm{ref}}=\mathcal{J}_0+\omega^2\mathcal{J}_1$. The parameter values used were $\mathcal{J}_0=13.4\ \hbar^2\mathrm{MeV}^{-1}$ and $\mathcal{J}_1=33.2\ \hbar^4\ \mathrm{MeV}^{-3}$. The results for each of the bands in $^{133}$Ce will be discussed in more detail in the following sections.

### B. Electromagnetic properties: $B(M1)/B(E2)$ values

Empirical ratios of reduced transition probabilities $B(M1;I\rightarrow I-1)/B(E2;I\rightarrow I-2)$ have been extracted for several of the bands in $^{133}$Ce. The values were obtained from the measured branching ratios for the $\Delta I=1$ and $\Delta I=2$ transitions, assuming the $E2/M1$ mixing ratio $\delta$ for the $\Delta I=1$ transitions is zero. This assumption is justified since the ratios are proportional to $(1+\delta^2)^{-1}$ with $\delta^2$ being typically only a few percent. The results are presented in Fig. 4 where they are compared to theoretical values obtained using the geometrical model[10] of Dönau and Frauendorf. The calculations used empirical $g$ factors for the $\pi h_{11/2}$ (+1.21), $\pi g_{7/2}$ (+0.74), $\nu h_{11/2}$ (−0.19), and $\nu s_{1/2}$ (−1.5) particles. These results will be discussed in more detail in subsequent sections, and will be used to assign specific configurations to some of the bands in $^{133}$Ce.

### C. The one-quasineutron bands

Bands are built on low-lying $I^\pi=\frac{1}{2}^+$ and $I^\pi=\frac{9}{2}^-$ states (bands 1 and 6, respectively, in Fig. 1). Both states were previously known,[13] but not the relative energy between them. From the present study, it is the $I^\pi=\frac{1}{2}^+$ level that is the ground state, being 39 keV lower than the $I^\pi=\frac{9}{2}^-$ level. The positive parity state is identified with the $[400]\frac{1}{2}^+$ Nilsson level which is derived from the $\nu s_{1/2}$ shell. Both signature components of the rotational band built on this state were observed. The measured $B(M1)/B(E2)$ values extracted for this band, shown in Fig. 4, agree well with calculated values for a pure $s_{1/2}$ single-quasineutron state. The small alignment $i_x$ for this configuration, shown in Fig. 3, is also consistent with this structure. An alternative assignment, based on a $d_{3/2}$ neutron orbital that is near the Fermi surface, can be ruled out for two reasons. First, the signature splitting of this one-quasineutron $d_{3/2}$ band would be opposite in phase, i.e., for the $d_{3/2}$ orbital the $\alpha=-\frac{1}{2}$ signature component is favored whereas for the $s_{1/2}$ orbital the $\alpha=+\frac{1}{2}$ component is favored, in agreement with experiment. Secondly, calculated $B(M1)/B(E2)$ ratios for the pure $d_{3/2}$ configuration are $10^3$ times smaller than the measured values.

Both signature components of the band built on the $I^\pi=\frac{9}{2}^-$ state were also observed. This level is identified with the $\nu h_{11/2}[514]\frac{9}{2}^-$ orbital. A large signature splitting, $\Delta e'\sim 100$ keV, that increases with rotational frequency, is observed between the two signature components, as shown in Fig. 3. This value is much larger than expected for the high-$\Omega$ $h_{11/2}$ neutron orbital in a prolate nucleus. Indeed cranked shell-model calculations for $\gamma=0°$ (prolate) and low frequencies ($\hbar\omega\leq 0.3$ MeV) show essentially no signature splitting for the $\nu h_{11/2}$ orbital. However, similar calculations for a triaxial nuclear shape ($\gamma\sim -20°$) can reproduce the large experimental signature splitting. The empirical

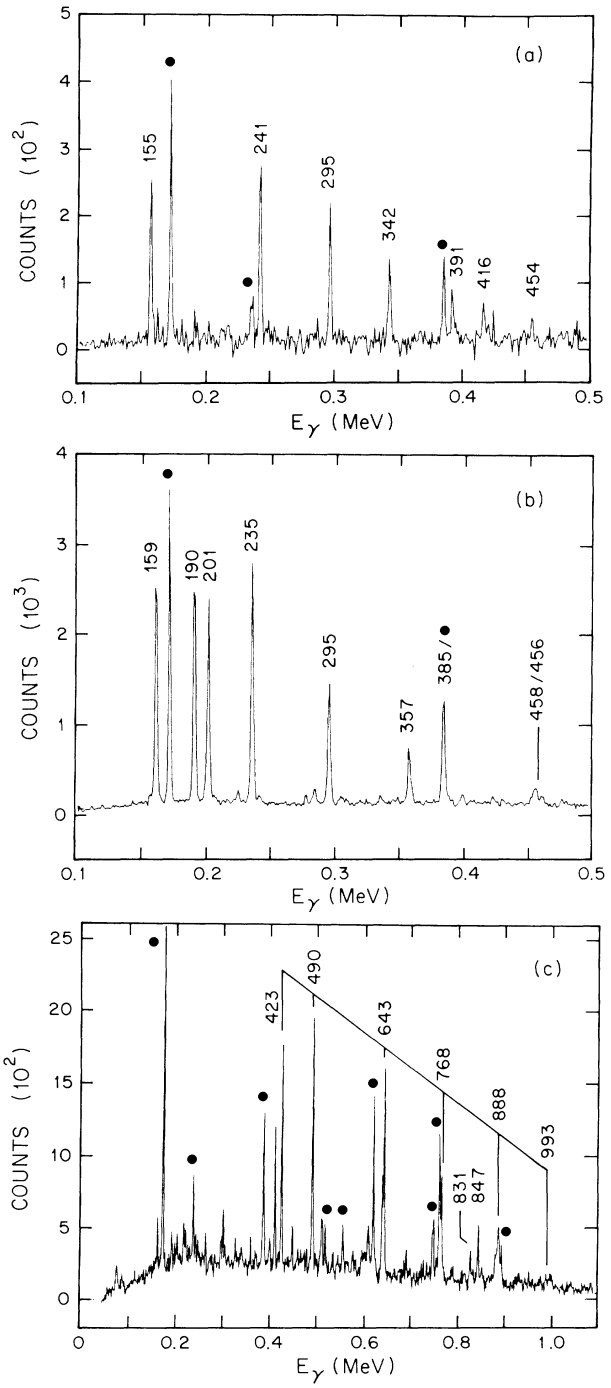


FIG. 2. (a) A gate set on the 1176 keV $\frac{25}{2}^- \rightarrow \frac{21}{2}^-$ transition. The labeled peaks (in keV) are associated with the $\nu h_{11/2} \otimes [\pi h_{11/2}]^2$ $\Delta I = 1$ band. Transitions in the $\nu h_{11/2}$ band are indicated by full circles. (b) A sum of gated spectra set on the 954 and 1269 keV transitions showing the $\Delta I = 1$ transitions (labeled in keV) in the positive-parity band built on the $\nu h_{11/2} \otimes \pi h_{11/2} \otimes \pi g_{7/2}$ configuration. Transitions in the $\nu h_{11/2}$ band are indicated by full circles. The 385 keV transition is a doublet. (c) A sum of gated spectra set on the 423, 490, 643, and 768 keV transitions. The labeled peaks (in keV) are associated with the $\Delta I = 2$ band built on the $\nu i_{13/2} \otimes [\pi h_{11/2}]^2$ configuration. Transitions in the $\nu h_{11/2}$ band are indicated by full circles.

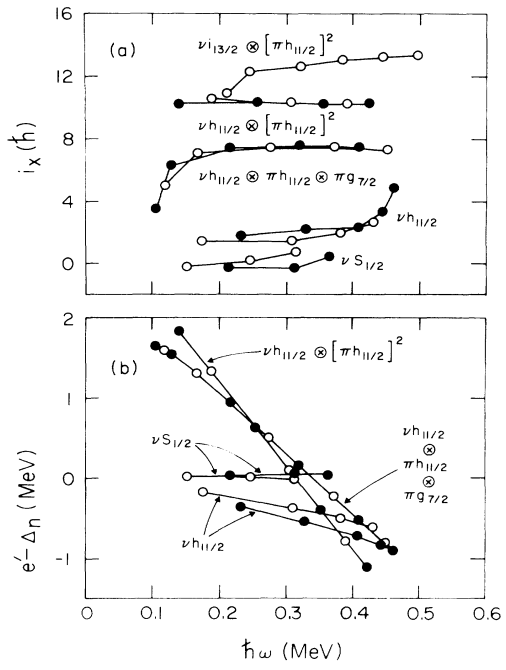


FIG. 3. Experimental alignments (a) and routhians (b) for most of the bands in $^{133}$Ce of signature $\alpha = -\frac{1}{2}$ (full circles) and $\alpha = +\frac{1}{2}$ (open circles). The alignment for the $\nu i_{13/2} \otimes [\pi h_{11/2}]^2$ band is also shown assuming a bandhead spin of $\frac{25}{2}$ and a $K$ value of $\frac{1}{2}$.

$B(M1)/B(E2)$ ratios extracted for this band exhibit a signature dependence, as shown in Fig. 4. Calculated ratios, including the experimental signature spitting for the $\nu h_{11/2}$ band, are also shown. These results, showing the characteristic sawtooth pattern, are in good agreement with the experimental values.

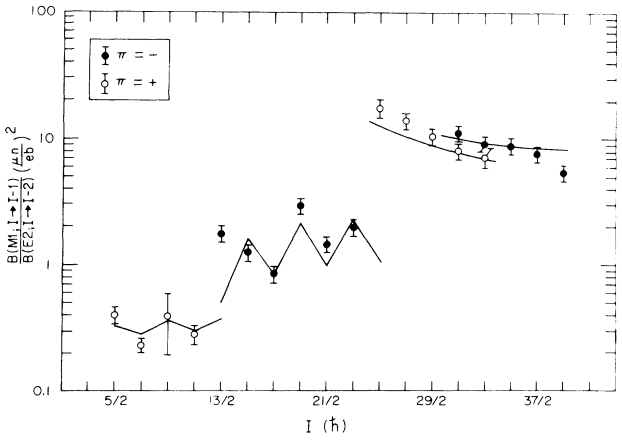


FIG. 4. Empirical $B(M1;I \rightarrow I-1)/B(E2;I \rightarrow I-2)$ ratios for one- and three-quasiparticle configurations in $^{133}$Ce. Negative parity bands ($\nu h_{11/2}$ at low spins, $\nu h_{11/2} \otimes [\pi h_{11/2}]^2$ at higher spins) are denoted by full circles, while positive parity bands ($\nu s_{1/2}$ at low spins, $\nu h_{11/2} \otimes \pi h_{11/2} \otimes \pi g_{7/2}$ at higher spins) are denoted by open circles. The full lines represent calculations for the various configurations using the semiclassical formalism of Dönau and Frauendorf (Ref. 10).

### D. The $\Delta I = 1$ sidebands

Four $\Delta I = 1$ sidebands, all with no signature spitting, were populated at higher spins. These bands are most likely built on three-quasiparticle configurations. For two of the bands (labeled 2 and 7 in Fig. 1), the weak $E2$ crossover transitions were observed making it possible to extract $B(M1)/B(E2)$ ratios. These two bands are similar to bands observed[3,9] in the N=75 isotones $^{135}$Nd and $^{137}$Sm. Comparisons to theoretical estimates of $B(M1)/B(E2)$ ratios for expected three-quasiparticle configurations have been used to assign configurations to these bands. The experimental and theoretical results are presented in Fig. 4.

The negative parity band (7 in Fig. 1) built on the $\frac{23}{2}^-$ level at 3238 keV has been identified with the configuration $\nu h_{11/2} \otimes [\pi h_{11/2}]^2$. Thus the band is based on a pair of rotationally aligned $h_{11/2}$ protons coupled to the odd $h_{11/2}$ neutron. The angular correlation ratios for the 1045.4 and 1176.5 keV transitions that link this band to the $\nu h_{11/2}$ band are consistent with a stretched $E2$ character. This three-quasiparticle band crosses both signatures of the $h_{11/2}$ one-quasineutron band at a frequency $\hbar\omega \sim 0.37$ MeV (see the experimental routhian plot of Fig. 3), which defines the crossing frequency for the alignment of the first pair of $h_{11/2}$ protons. The crossing is associated with an increase in the alignment $\Delta i_x \sim 9\ \hbar$ (Fig. 3) relative to that of the $\nu h_{11/2}$ band, as expected for a pair of rotationally-aligned $h_{11/2}$ protons. The protons, from the lower $h_{11/2}$ midshell, exert a strong $\gamma$-driving force on the nuclear core opposite to that of the odd neutron. The protons favor a near-prolate shape ($\gamma \sim 0°$) and induce a shape change from the discussed triaxial shape ($\gamma \sim -20°$) below the alignment to a near-prolate shape. For this $\gamma \sim 0°$ prolate shape, the signature splitting due to the odd neutron falls to zero. This is evident in the experimental routhian plots of Fig. 3 and is consistent with CSM calculations for a prolate shape.

A comparison of the experimental crossing frequencies for the first pair of $h_{11/2}$ protons in the yrast $h_{11/2}$ neutron bands of the $N=75$ isotones $^{133}$Ce, $^{135}$Nd, and $^{137}$Sm is shown in Table II. The values for each nucleus are larger than CSM prediction ($\hbar\omega_c \sim 0.3$ MeV) for a prolate nucleus of moderate quadrupole deformation $\beta = 0.2$. However, the high crossing frequencies are reproduced for the triaxial shape $\gamma \sim -20°$ extracted from the signature splitting below the proton alignment. The observed signature splittings in the one-quasineutron $h_{11/2}$ bands, at $\hbar\omega = 0.3$ MeV, are also shown. These relatively large values complete a consistent data set defining the significant triaxial shape for each nucleus at low spin.

This proton alignment in $^{133}$Ce is also associated with an increase in the $B(M1)/B(E2)$ ratios; an increase by a factor $\sim 5$ is seen in Fig. 4. Although a decrease in the $E2$ transition rates is expected for the shape change $\gamma = -20° \rightarrow \gamma = 0°$ [$B(E2; I \rightarrow I-2) \propto \cos^2(\gamma + 30°)$], the large $B(M1)/B(E2)$ ratios extracted for the $\nu h_{11/2} \otimes [\pi h_{11/2}]^2$ band are mainly due to enhanced $M1$ transitions. This effect can easily be understood in the geometrical model of Dönau and Frauendorf.[10] The opposite sign of the $g$ factors for the $h_{11/2}$ proton and $h_{11/2}$ neutron increases the component of the magnetic moment $\mu$ perpendicular to the total spin I of the nucleus. The $M1$ transition rate, proportional to the square of this perpendicular component, is thus increased. Enhanced $B(M1)$ values generally occur for mixed neutron-proton configurations. In addition to other odd-$N$ nuclei in this mass region, similar effects are seen in heavier odd-$Z$ rare earth nuclei, for example[16] in $^{159}$Tm, where band crossings in $h_{11/2}$ proton bands are attributed to $i_{13/2}$ neutrons.

TABLE II. A comparison of the band-crossing frequencies for the alignment of $h_{11/2}$ protons observed in both signatures of the $\nu h_{11/2}$ yrast bands (Refs. 3 and 9) of several $N=75$ isotones. The quoted values, extracted from the experimental routhians, are accurate to ±0.002 MeV. The signature splitting between the two components of the $\nu h_{11/2}$ band, extracted at $\hbar\omega = 0.3$ MeV, is also shown for each nucleus. These values are accurate to ±0.005 MeV.

| Nucleus | Signature component | $\hbar\omega_c$ (MeV) | Signature splitting (MeV) |
|---|---|---|---|
| $^{133}$Ce | $\alpha = -\frac{1}{2}$ | 0.378 | 0.120 |
| | $\alpha = +\frac{1}{2}$ | 0.359 | |
| $^{135}$Nd | $\alpha = -\frac{1}{2}$ | 0.336 | 0.115 |
| | $\alpha = +\frac{1}{2}$ | 0.318 | |
| $^{137}$Sm | $\alpha = -\frac{1}{2}$ | 0.351 | 0.110 |
| | $\alpha = +\frac{1}{2}$ | 0.331 | |

The positive parity band (2 in Fig. 1) built on the $\frac{15}{2}^+$ state at 1899 keV is also based on a three-quasiparticle configuration. In this case, the two protons are in different orbitals; the structure assigned to this band is the $\nu h_{11/2} \otimes \pi h_{11/2} \otimes \pi g_{7/2}$ configuration. Again, this configuration is prolate because the observed signature splitting for the $h_{11/2}$ neutron is zero, which implies that the $h_{11/2}$ proton $\gamma$-driving force is dominant. A value of $K = \frac{15}{2}$ was used for this configuration in extracting the alignment $i_x$ and for calculating the $B(M1)/B(E2)$ values. There is excellent agreement between experiment and theory as evident in Fig. 4. As discussed above, relatively large $B(M1)/B(E2)$ ratios are extracted for this positive-parity band because of the mixed neutron-proton configuration. The angular correlation ratios of the 954.0 and 1269.3 keV transitions that connect this band to the $\nu h_{11/2}$ band are consistent with stretched dipole character; hence they have been assigned an $E1$ multipolarity.

As stated earlier, band structures similar to the two discussed above (2 and 7 in Fig. 1) have been observed[3,9] in the isotones $^{135}$Nd and $^{137}$Sm. However, the $\Delta I = 1$ bands built on the states at 2417 and 2746 keV in $^{133}$Ce (labeled 3 and 4, respectively, in Fig. 1) have no analogous in the heavier isotones. The strong $\Delta I = 1$ transitions and lack of signature splitting implies that these two bands are built on prolate three-quasiparticle configurations containing both protons and neutrons. A

possible configuration for one of these bands is the same as that for the positive-parity band (2 in Fig. 1) built on the $\frac{15}{2}^+$ state at 1899 keV, i.e., the $\nu h_{11/2}\otimes\pi h_{11/2}\otimes\pi g_{7/2}$ configuration. In this case, the favored signature of the $h_{11/2}$ proton orbital is coupled to the unfavored signature of the $g_{7/2}$ proton orbital (as opposed to the favored component); these protons are then coupled to both signatures of the $h_{11/2}$ neutron orbital giving rise to a rotational band with no signature splitting, i.e., a $\Delta I=1$ band. Similar structures can also be created by coupling the unfavored signature component of the $h_{11/2}$ proton to the same two particles. In each case, it is the absence of signature splitting of the high-$\Omega$ neutron orbital for near-prolate shapes ($\gamma\sim0°$) that gives rise to a $\Delta I=1$ band

### E. The $\Delta I=2$ sideband

The $\Delta I=2$ band, consisting of the 423.1, 489.4, 643.0,... keV transitions (labeled 5 in Fig. 1), is a decouple band of only one signature component built on a low-$\Omega$ neutron state. Nilsson single-particle systematics show two possible neutron orbitals near the Fermi surface. These are the positive-parity $[660]\frac{1}{2}^+$ and negative-parity $[541]\frac{1}{2}^-$ orbitals derived from the $\nu i_{13/2}$ and $\nu f_{7/2}$ shells, respectively. The $i_{13/2}$ orbital will be favored over the $f_{7/2}$ orbital at high frequencies because of the higher $j$ value. Furthermore, there is recent evidence[17] for the presence of the $\nu i_{13/2}$ $[660]\frac{1}{2}^+$ orbital in the level structure of the neighboring odd-N $^{135}$Sm nucleus. The $\Delta I=2$ band structure most probably also contains a pair of rotationally aligned $h_{11/2}$ protons, which are the most easily aligned particles. Thus, the band is most likely built on the prolate $\nu i_{13/2}\otimes[\pi h_{11/2}]^2$ three-quasiparticle configuration.

It was not possible to uniquely place this band in the decay scheme in Fig. 1. The band appears to decay to the lower-lying states via many pathways. One decay path is into the lower members of the positive-parity three-quasiparticle band via the 831.1 keV and other transitions. A second path is a decay to the $\frac{23}{2}^-$ level which in turn decays to the $\nu h_{11/2}$ band via the 1089.0 keV $E2$ transition. Yet a third decay path may occur directly into the $\nu h_{11/2}$ band via the 847.0 keV transition. The angular correlation ratio for this transition is consistent with a stretched $E1$ assignment. This would then establish the bandhead spin of the $\Delta I=2$ band as $\frac{25}{2}$. The alignment of this band, shown in Fig. 3, was calculated assuming this value for the bandhead spin and is consistent with the proposed three-quasiparticle structure.

The extracted dynamical moment of inertia ($\mathcal{J}^{(2)}=dI_x/d\omega$) for the $\Delta I=2$ $\nu i_{13/2}\otimes[\pi h_{11/2}]^2$ band is $\sim25\%$ larger than those extracted for the other three-quasiparticle $\nu h_{11/2}\otimes[\pi h_{11/2}]^2$ and $\nu h_{11/2}\otimes\pi h_{11/2}\otimes\pi g_{7/2}$ bands (2 and 7) in the frequency range $0.30\le\hbar\omega\le0.45$ MeV. This effect can also be seen in the alignment plot of Fig. 3. The reference moment of inertia was fitted to the $\nu h_{11/2}\otimes[\pi h_{11/2}]^2$ band; both this band and the $\nu h_{11/2}\otimes\pi h_{11/2}\otimes\pi g_{7/2}$ band show constants alignments whereas that for the $\nu i_{13/2}\otimes[\pi h_{11/2}]^2$ band increases slightly with rotationally frequency, indicating a larger moment of inertia. Since all three of these bands are built on prolate three-quasiparticle structures, the larger moment of inertia is most likely caused by an increased quadrupole deformation $\beta$, and not by a reduction of the pairing due to blocking of quasiparticle orbitals. The shape driving ($\beta$) effect of quasiparticle orbitals, proportional to the slope $dE/d\beta$ of the Nilsson levels, is greatest for the low-$\Omega$ components of shell and is hence expected to be strong for the $[660]\frac{1}{2}^+$ orbital.

Although the moment of inertia of the $\nu i_{13/2}\otimes[\pi h_{11/2}]^2$ band ($\mathcal{J}^{(2)}\sim33\ \hbar^2\ \mathrm{MeV}^{-1}$) is larger than the other three-quasiparticle bands in $^{133}$Ce, the value is only $\sim50\%$ of the values extracted for superdeformed bands[18,19] in neighboring odd-$N$ nuclei. The superdeformed bands ($\beta\sim0.35$–$0.4$) in this mass region are believed[20] to be built on multi-quasiparticle configurations involving a $\beta$-driving $\nu i_{13/2}$ orbital. The present results for $^{133}$Ce indicate that the driving force of the $\nu i_{13/2}$ $[660]\frac{1}{2}^+$ orbital is sufficient to increase the quadrupole deformation $\beta$ beyond a value of $\beta\sim0.2$, the typical value for nuclei in the vicinity of $^{133}$Ce, but further quasiparticle excitations are required to drive the nucleus to the superdeformed shape with $\beta\sim0.4$. The lifetime data place an upper limit of $t_{1/2}<8$ ns for the bandhead of the $\Delta I=2$ band in $^{133}$Ce which indicates that the deformation cannot be too dissimilar to the values in the other rotational bands at low spins.

## IV. CONCLUSIONS

Several rotational bands have been populated in the odd-neutron $^{133}$Ce nucleus. At low spins, the $\nu h_{11/2}$ yrast band is triaxial because of the shape-driving effect of the high-$\Omega$ neutron from the upper $h_{11/2}$ midshell. This is manifest by a large signature splitting in this band and a high alignment frequency for the first pair of $h_{11/2}$ protons. At a frequency of $\hbar\omega_c\sim0.37$ MeV, a pair of low-$\Omega$ protons from the lower $h_{11/2}$ midshell align. The shape-driving effect of this pair of protons, being opposite to that of the neutron, changes the nuclear shape to a prolate ($\gamma\sim0°$) shape. At the $\gamma\sim0°$ prolate shape, the signature splitting of the $h_{11/2}$ neutron orbital approaches zero. A second three-quasiparticle band of similar characteristics, i.e., strong $M1$ transitions and no signature splitting, has been assigned the $\nu h_{11/2}\otimes\pi h_{11/2}\otimes\pi g_{7/2}$ configuration by comparison of experimental and theoretical $B(M1)/B(E2)$ ratios. Similar bands have been observed in the isotones $^{135}$Nd and $^{137}$Sm. Two additional $\Delta I=1$ bands were observed in $^{133}$Ce, most probably based on prolate mixed proton-neutron configurations. In these bands the crossover $E2$ transitions were not observed.

A strong $\Delta I=2$ band was also populated, which is believed to be based on the $\nu i_{13/2}\otimes[\pi h_{11/2}]^2$ configuration. The maximal signature splitting of the low-$\Omega$ $i_{13/2}$ $[660]\frac{1}{2}^+$ orbital allowed the observation of only the

favored signature component ($\alpha = +\frac{1}{2}$) of this configuration. This structure possibly has a larger quadrupole deformation than the other bands seen at low spins in $^{133}$Ce, and is related to the $\nu i_{13/2} \otimes [\pi h_{11/2}]^n$ configuration which has been invoked to explain the observed superdeformed bands of this mass region.

*Note added in proof.* Although cranked shell model (CSM) calculations with the standard Nilsson parameters $\kappa$ and $\mu$ suggest the $\nu i_{13/2} \otimes [\pi h_{11/2}]^2$ configuration as the structure of the $\Delta I = 2$ band, similar calculations using the modified parameters of Bengtsson and Ragnarsson [T. Bengtsson and I. Ragnarsson, Nucl. Phys. **A436**, 14 (1985)] favor the $\nu f_{7/2} \otimes [\pi h_{11/2}]^2$ structure. Recent calculations by Zhang (J.-Y. Zhang, private communication) have indicated that both of these possible configurations possess $\beta \sim 0.21$ as compared to $\beta \sim 0.17$ for the $\nu h_{11/2}$ yrast band. However, the relatively larger alignment observed for the $\Delta I = 2$ decoupled band, shown in Fig. 3, favors the $\nu i_{13/2}$ orbital. The predicted CSM alignment for the $\nu i_{13/2} \otimes [\pi h_{11/2}]^2$ configuration is $i_x \sim 14.6\hbar$, while $i_x \sim 11.8\hbar$ is predicted for the $\nu f_{7/2} \otimes [\pi h_{11/2}]^2$ structure and $i_x \sim 11.2\hbar$ for the $\nu h_{11/2} \otimes [\pi h_{11/2}]^2$ structure.

## ACKNOWLEDGMENTS

This work was in part supported by the National Science Foundation. One of us (S.S.) acknowledges receipt of a K. K. Leung Fellowship through the Committee of Educational Exchange with China.

*Present address: Lawrence Berkeley Laboratory, University of California, Berkeley, CA 94720.

†Permanent address: Institute of Nuclear Research, Shanghai, China.

[1]G. Andersson, S. E. Larsson, G. Leander, P. Möller, S. G. Nilsson, I. Ragnarsson, S. Åberg, R. Bengtsson, J. Dudek, B. Nerlo-Pomorska, K. Pomorski, and Z. Szymański, Nucl. Phys. **A268**, 205 (1976).

[2]R. Aryaeinejad, D. J. G. Love, A. H. Nelson, P. J. Nolan, P. J. Smith, D. M. Todd, and P. J. Twin, J. Phys. G **10**, 955 (1984).

[3]W. F. Piel, Jr., C. W. Beausang, D. B. Fossan, L. Hildingsson, and E. S. Paul, Phys. Rev. C **35**, 959 (1987).

[4]I. Ragnarsson, A. Sobiczewski, R. K. Sheline, S. E. Larsson, and B. Nerlo-Pomorska, Nucl. Phys. **A233**, 329 (1974).

[5]Y. S. Chen, S. Frauendorf, and G. A. Leander, Phys. Rev. C **28**, 2437 (1983).

[6]G. A. Leander, S. Frauendorf, and F. R. May, in *Proceedings of the Conference on High Angular Momentum Properties of Nuclei, Oak Ridge, 1982,* edited by N. R. Johnson (Harwood Academic, New York, 1983), p. 281.

[7]S. Frauendorf and F. R. May, Phys. Lett. **125B**, 245 (1983).

[8]R. Bengtsson and S. Frauendorf, Nucl. Phys. **A327**, 139 (1979).

[9]R. Ma, C. W. Beausang, E. S. Paul, W. F. Piel, Jr., S. Shi, N. Xu, and D. B. Fossan, Bull. Am. Phys. Soc. **32**, 1096 (1987).

[10]F. Dönau and S. Frauendorf, in *Proceedings of the Conference on High Angular Momentum Properties of Nuclei, Oak Ridge, 1982,* edited by N. R. Johnson (Harwood Academic, New York, 1983), p. 143; F. Dönau, Niels Bohr Institute (University of Copenhagen) Report NBI-ZFK 86-36, 1985.

[11]L. Hildingsson, C. W. Beausang, D. B. Fossan, W. F. Piel, Jr., A. P. Byrne, and G. D. Dracoulis, Nucl. Instrum. Methods A **252**, 91 (1986).

[12]K. S. Krane, R. M. Steffen, and R. M. Wheeler, Nucl. Data Tables A **11**, 351 (1973).

[13]F. Rösel, H. M. Fries, K. Alder, and H. C. Pauli, At. Data Nucl. Data Tables **21**, 91 (1978).

[14]*Tables of Isotopes,* 7th ed., edited by C. M. Lederer and V. S. Shirley (Wiley, New York, 1978).

[15]S. M. Harris, Phys. Rev. **138**, B509 (1965).

[16]A. J. Larabee, L. H. Courtney, S. Frauendorf, L. L. Riedinger, J. C. Waddington, M. P. Fewell, N. R. Johnson, I. Y. Lee, and F. K. McGowan, Phys. Rev. C **29**, 1934 (1983).

[17]S. M. Mullins, R. Wadsworth, J. M. O'Donnell, P. J. Nolan, A. J. Kirwan, P. J. Bishop, M. J. Godfrey, and D. J. G. Love, J. Phys. G **13**, L201 (1987).

[18]E. M. Beck, F. S. Stephens, J. C. Bacelar, M. A. Delaplanque, R. M. Diamond, J. E. Draper, C. Duyar, and R. J. McDonald, Phys. Rev. Lett. **58**, 2182 (1987).

[19]R. Wadsworth, A. Kirwan, D. J. G. Love, Y.-X. Luo, J.-Q. Zhong, P. J. Nolan, P. J. Bishop, M. J. Godfrey, R. Hughes, A. N. James, I. Jenkins, S. M. Mullins, J. Simpson, D. J. Thornley, and K. L. Ying, J. Phys. G **13**, L207 (1987).

[20]Y. S. Chen, private communication.